applied sciences

MDPI

Article

Long- and Short-Term Stability of All Polarization-Maintaining Thulium Doped Passively Mode-Locked Fiber Lasers with Emission Wavelengths at 1.95 μm and 2.07 μm

Christian Cuadrado-Laborde [1,2,*], Jose L. Cruz [3], Antonio Díez [3] and Miguel V. Andrés [3]

[1] Institute of Physics Rosario IFIR (CONICET-UNR), Blvr. 27 de Febrero 210bis, Rosario S2000EZP, Argentina
[2] Facultad de Química e Ingeniería, Pontificia Universidad Católica Argentina, Av. Pellegrini 3314, Rosario 2000, Argentina
[3] Laboratory of Fiber Optics, Department of Applied Physics, Institut de Ciencia dels Materials (ICMUV), University of Valencia, c/Dr. Moliner 50, 46100 Burjassot, Valencia, Spain
* Correspondence: christiancuadrado@uca.edu.ar

Featured Application: cutting/engraving/welding of plastics, laser scalpels, eye-safe light detection and ranging (LIDAR), remote sensing, and real-time spectroscopy.

Abstract: In this work, we compare the operation of a passively modelocked polarization-maintaining emission in two thulium-doped fiber lasers pumped at 1561 nm, with emission at wavelengths of 1.951 μm in one case and 2.07 μm in the other. We obtained a sequence of light pulses at 15.6 MHz, whose temporal width was 81 ps at 1.95 μm, and a sequence of light pulses at 13.1 MHz, whose temporal width was 94 ps at 2.07 μm. Finally, we also measured the long-term stability of this setup during a 24-h operation, as well as the short-term stability in a simulated harsh environment. The results confirm the superior performance of fiber laser systems with a fully polarization-maintaining design.

Keywords: thulium doped fibers; fiber lasers; passive mode-locking; polarization-maintaining

Citation: Cuadrado-Laborde, C.; Cruz, J.L.; Díez, A.; Andrés, M.V. Long- and Short-Term Stability of All Polarization-Maintaining Thulium Doped Passively Mode-Locked Fiber Lasers with Emission Wavelengths at 1.95 μm and 2.07 μm. *Appl. Sci.* **2023**, *13*, 1981. https://doi.org/10.3390/app13031981

Academic Editor: Maria Michalska

Received: 23 November 2022
Revised: 2 January 2023
Accepted: 31 January 2023
Published: 3 February 2023

1. Introduction

Free-space communication [1], light detection and ranging (LIDAR), or gas detection systems [2,3] would take advantage of laser systems operating at 2 μm because they are "eye safe" compared to conventional systems operating at shorter wavelengths. The strong water absorption in this wavelength range also makes these laser systems ideal for medical applications [4,5], such as tissue ablation [6], dermatology [7], and scalpels [8]. These laser systems have also shown promise for low-latency interconnection using hollow-core fibers [9], as well as for cutting and welding polymers [10].

There are already some proposals for all-fiber modelocked laser systems that emit below [11–16] or above [17–25] 2 μm and use a thulium doped fiber (TDF) as the medium gain. These proposals for a mode-locking mechanism primarily rely on nonlinear polarization rotation (NPR) [11,20,25], nonlinear optical loop mirrors (NOLM) [14–19], nonlinear amplifying loop mirrors (NALM) [12], non-semiconductor saturable absorbers (NSA) [13,21–23], or, much less frequently, semiconductor saturable absorbers (SESA) in either transmission or reflection (SESAM, semiconductor saturable absorber mirrors) [22,24]. In an ultralong cavity, NPR, NOLM, and NALM are prone to overdrive, and all depend heavily on the polarization and phase evolution of the optical pulse. For this reason, most of these proposals use polarization controls that require multiple adjustments and the uncertainty of self-start. In addition, the operating wavelength often varies depending on the polarization of the resonator and pump power, which could be a serious problem in some applications. Single-walled carbon nanotubes [13], iron-doped carbon nitride nanosheets [21], and MoS_2 [23] are examples of NSAs that are still at an early stages of technology development

and whose behavior has not yet been tested under challenging conditions. SESAMs are a mature technology that are inherently compatible with polarization-maintaining (PM) cavities, unlike other proposals based on polarization evolution, nonlinear optical loop mirrors, and similar solutions.

Although there are other proposals that use holmium-doped fibers [26], in this work, we focus on laser systems operating in the 2 μm range whose medium gain is a thulium-doped fiber. However, there are some differences between the emission cross sections of the two medium gains, with a maximum for TDFs at 1.85 μm [27] and holmium doped fibers (HDFs) at 2.02 μm [28]. TDFs can be pumped at 0.79 or 1.56 μm [29], making pumping sources easily accessible. In contrast, HDFs require less accessible pumping sources with emissions at 1.1 or 1.9 μm [30]. Since the emission and absorption bands strongly overlap, reabsorption is a second problem for HDFs that does not occur for TDFs.

Therefore, our goal in this work is to compare the passively modelocked emission using a TDF resonantly pumped in C-band as the medium gain and a SESAM as the mode-locker at both the common emission wavelength of 1.95 μm and at the less common (for a TDF) emission wavelength of 2.07 μm. Since robustness to environmental effects is a must for practical applications, we designed both lasers in a fully polarization-maintaining cavity. Both lasers have been properly characterized, and we have tested both the long-term stability of this setup in 24-h operation and the short-term stability in a simulated harsh environment.

2. Experimental Procedure

The experimental setup, shown in Figure 1a, was essentially identical for the two lasers studied in this work. First, we sketch the configuration of the Fabry–Pérot resonator, whose emission was focused at 1.95 μm. At one end we used a highly reflective PM fiber Bragg grating (PM FBG 1, >99% reflectance, λ_B = 1951 nm, and 140 pm bandwidth at −3 dB) and at the other end a SESAM (relaxation time constant of 10 ps and a high reflectance bandwidth between 1900 and 2080 nm). On the other side, Figure 1b shows the measured spectrum of PM FBG. These spectra contain two peaks representing the slow and fast axes and are the result of measuring PM FBG with a 2 μm unpolarized amplified spontaneous emission light source. The medium gain was a PM TDF from Nufern® (length of 2 m, PM-TSF 9/125, 0.15 numerical aperture, cutoff wavelength of 1750 nm, and 9 ± 2 dB/m absorption at 1180 nm). However, to protect the SESAM from excess pump power that was not absorbed by the medium gain, we also incorporated a PM wavelength division multiplexer into the system (PM WDM, 1550/1950 nm, with an insertion loss from the transmit port to the common port <0.6 dB at 1950 nm, and an insertion loss from the reflect port to the common port <0.5 dB at 1550 nm). A dichroic mirror was then used to redirect the excess pump power back into the cavity. A PM fiber optic coupler (PM OFC, 90/10, with a central wavelength of 1950 nm and a blocked fast axis) was then added to complete the cavity. As for the pump source, indirect pumping into the $_3F^4$ energy level (peak absorption at 790 nm) is quite common, while direct in-band pumping into the $_3H^4$ energy level (peak absorption at 1610 nm) is known for near-optimal performance [31]. We chose the latter because it has much higher efficiency. Consequently, a high-power laser diode (7.7 W) emitting at 976 nm was used to pump a custom continuous wave (CW) laser emitting at 1561 nm with a maximum power of 820 mW. At a laser threshold of 47 mW, the pumping unit's slope efficiency was 10.57 ± 0.08%. This pump power was injected into the resonator through the remaining port of the PM FBG. Finally, to prevent unwanted reflections in the resonator, a second optical isolator (PM I, central wavelength of 1950 ± 20 nm, peak isolation of 28 dB, and insertion loss of 0.6 dB) was inserted into the 10% port of the PM OFC, where the output power was obtained.

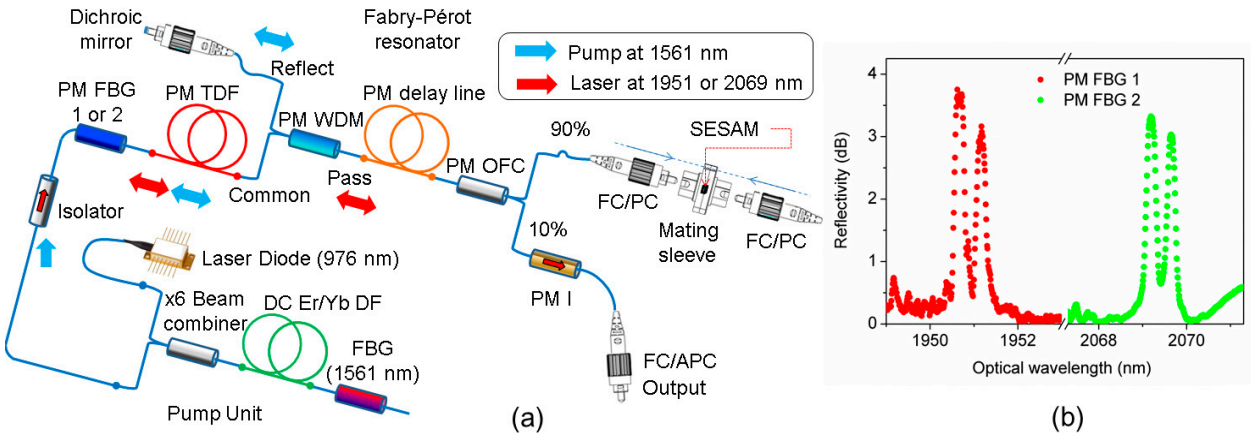

Figure 1. (**a**) Structure of the fiber laser. (**b**) Optical spectra of PM FBG 1 tuned to 1.951 µm (red dots), and PM FBG 2 tuned to 2.07 µm (green dots).

The design of the second laser was largely the same as that of the laser emitting at 1.95 µm; only the components that were incompatible with the new emission wavelength were changed [32]. The design includes PM WDM (1550/2070 nm, with an insertion loss from the transmit port to the common port <0.6 dB at 2070 nm and from the reflect port to the common port <0.5 dB at 1550 nm), a new 90/10 PM OFC (fast axis blocking and central wavelength 2070 nm), a new optical isolator (PM I, peak isolation of 28 dB and central wavelength at 2070 ± 20 nm), and a longer PM TDF of 3.2 m (instead of the 2 m originally used for emission at 1.951 µm). This last adjustment was necessary because the emission maximum for the $^3F_4 \rightarrow {}^3H_6$ transition occurs at an emission wavelength of 1.837 µm, which is a long way away at 2.07 µm. Consequently, the emission cross section decreases by 72%, compared to the maximum at 1.837 µm [33]. In addition, there is a higher loss at the emission wavelength of 2.07 µm than at 1.951 µm. For both reasons, we found it necessary to compensate with a longer thulium-doped fiber at the emission wavelength of 2.07 µm than at 1.951 µm. Finally, both lasers were characterized using a real-time oscilloscope with a bandwidth of 13 GHz, a sampling oscilloscope with a bandwidth of 63 GHz, InGaAs photodetectors with rise/fall times of 28 ps, an optical spectrum analyzer with a resolution of 50 pm, an electrical spectrum analyzer with a maximum bandwidth of 10 GHz and a maximum resolution of 1 Hz, and finally a pyroelectric sensor with the capability to record the output power of the studied laser system at different sampling rates.

The length of the resonator was 6.25 m for the 1.95 µm tuning and 7.89 m for the 2.07 µm tuning. For the emission wavelengths of 1.951 µm and 2.07 µm, the calculated total chromatic dispersion and losses per round trip were -1 ps^2 and 5.8 dB, and -1.58 ps^2 and 6 dB, respectively, i.e., anomalous in both cases.

3. Discussion

At both emission wavelengths, the lasers exhibited self-starting stable mode-locking when the diode laser power exceeded a predetermined threshold. We begin with the description of the 1.95 µm laser. When the laser diode output power reaches 2.5 W, stable mode-locking starts; see Figure 2a. When this pump power is exceeded, the output light train experiences the usual amplitude modulation over the modelocked train. The output light pulse train at 15.6 MHz and the corresponding radio frequency (RF) spectrum centered on this fundamental frequency (corresponding to a resonator length of 6.25 m) are shown in Figure 2a,b respectively. The stability of this mode-locking regime is evidenced by the high extinction ratio in the RF spectrum (65 dB, measured with a resolution bandwidth of 10 Hz). Figure 2c shows the output light pulse in detail. A full width at half maximum (FWHM) measurement of 81 ps identified a secant hyperbolic profile. There is also a ripple at the trailing edge, but this is only a side effect of the photodetector transfer function [34]. Figure 2d shows the output spectrum of this laser, which we also measured. A single peak

in the spectrum has a bandwidth of 50 pm at 3 dB, which is approximately the resolution limit of our optical spectrum analyzer (50 pm) [35]. Finally, the measured average output power after the PM isolator was 230 µW, so the peak power of the pulsed emission is about 100 mW. This corresponds to a laser efficiency of about 0.1%, which is consistent with previous work using TDF [36].

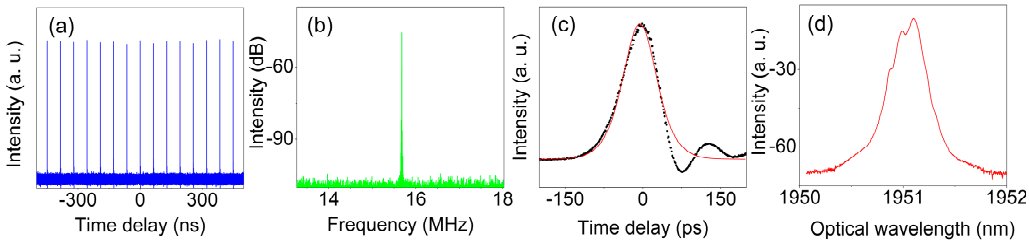

Figure 2. Laser with emission at 1.95 µm. (**a**) Pulse train at the fundamental repetition rate. (**b**) RF spectrum showing the first harmonic. (**c**) Waveform of the single pulse in the time domain (solid black points) and its corresponding fitting by a square hyperbolic secant profile (solid red curve). (**d**) Measured spectrum of the output.

We continue with the characterization of the laser emitting at the optical wavelength of 2.07 µm. When the output power of the laser diode is 3 W, the laser also exhibits self-starting stable mode-locking; see Figure 3a. At this pump power, the laser delivers one pulse per round trip at a repetition rate of 13.084 MHz, which is the reciprocal of the expected round trip time for a 7.89 m Fabry–Pérot resonator. Mode-locking is maintained when the laser diode emits a pump power greater than 3 W, but the laser emits multiple pulses per round trip. For example, when the laser diode output power reaches 4.1 W, two pulses are generated per round trip, and so on until the maximum available pump power is reached. Soliton lasers typically exhibit such behavior. The output sequence of light pulses at 13.084 MHz and the corresponding spectrum from RF, both shown in Figure 3a,b. Another indication of the stability of this mode-locking regime is the high extinction ratio in the RF spectrum (up to 80 dB, measured with a resolution bandwidth of 1 Hz). Figure 3c shows a detailed illustration of the waveform of a single pulse in the time domain. The curve has a FWHM of 94 ps and fits well with a hyperbolic square secant profile (also shown). These output light pulses are slightly wider compared to our earlier finding with emission at 1.95 µm. As an example, we can compare these results with Ref. [36], where a modelocked fiber laser was presented that uses a TDF as medium gain and an NSA as the mode-locker and is also pumped in the C-band, but with a fiber resonator not polarization-preserved. In this case, the FHWM of the pulse width is considerably shorter (~1.4 ps). This is the result of not using ad hoc filtering within the cavity, except of course for those intrinsically associated with the various elements (couplers, WDMs, etc.). In our case, there is strong filtering by the FBG, see Figure 1a, which reduces the spectral bandwidth of the output pulse while broadening the pulse in the time domain.

Since the repetition rate was almost the same, a similar nonlinear parameter is expected but with a larger dispersion, resulting in a wider pulse width in this case. This result is consistent with previous theoretical studies for soliton lasers that predicted an increase in pulse width with increasing chromatic dispersion for a fixed nonlinear parameter [37,38]. Figure 3d shows the measured output spectrum of this laser. The expected spectral bandwidth for a transform-limited pulse is represented by a single peak in the spectrum at 2.07 µm with a 3 dB bandwidth of 70 pm. On the other hand, 450 µW was the average output power measured after the PM isolators. Moreover, an average power of 10.4 mW can be obtained in the cavity, while the peak power in the cavity is 7.94 W due to the 94 ps pulse width.

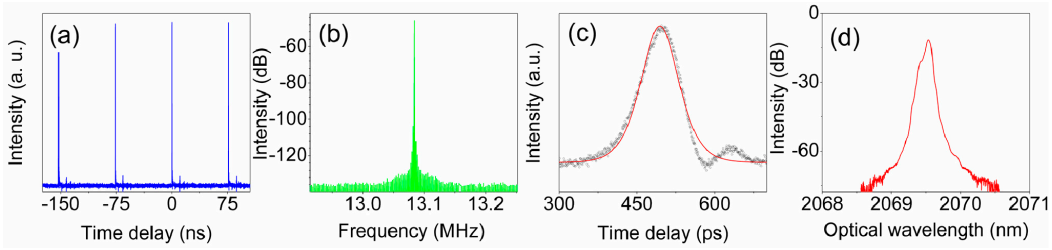

Figure 3. Laser with emission at 2.07 µm. (**a**) Pulse train at the fundamental repetition rate. (**b**) RF spectrum showing the first harmonic. (**c**) Waveform of the single pulse in the time domain (solid black points) and its corresponding fitting by a square hyperbolic secant profile (solid red curve). (**d**) Measured spectrum of the output.

Fiber laser operation is generally susceptible to various external disturbances such as thermal variations, motion, vibration, and other parameters that may contribute to polarization change due to motion or stress. This significantly affects the reliability and performance of the laser unless polarization is fully maintained in the cavity through the use of polarization-maintaining fibers and components [39–42]. Therefore, we determined both the long-term and short-term stability of this fully polarization-maintaining configuration using the laser with an emission of 1.95 µm as an example; see Figure 1a. The long-term stability was investigated by continuously recording the output power and spectrum during a 24 h operation; see Figure 4a,b. Thus, the laser was operated continuously without any support or monitoring and without controlling the room temperature (16 °C temperature variation during the 24 h). Nevertheless, the laser operated continuously, and the output power showed only a small variation of only 4%; see Figure 4a. This small power fluctuation could be, among others, a consequence of the temperature dependence of the reflection of the saturable absorber [39]. The evolution of the output spectrum recorded every 1/2 h during the 24 h operation is shown in Figure 4b (for clarity, we preferred to include only the spectra recorded every 3 h). It can be seen that there are no significant changes in the output spectrum, except for a small shift of 0.2 nm in the emission wavelength, which can be understood as a consequence of the thermal drift of the FBG, since the room temperature was not controlled. Of course, this spectral shift could be minimized if needed by fixing the reflection wavelength of the FBG by controlling its temperature. Finally, short-term stability in a harsh environment was simulated by recording the output power while the table on which the laser was mounted was subjected to strong random vibrations measured with an accelerometer. It is noteworthy that the laser ran without interruption, and the average power standard deviation was only 1.2%. This long- and short-term stability is to be expected with an all-fiber design that fully retains polarization. Furthermore, the use of a SESAM as a mode-locker and a fully polarization-maintaining resonator ensures this insensitivity to temperature variations and mechanical vibration, as shown.

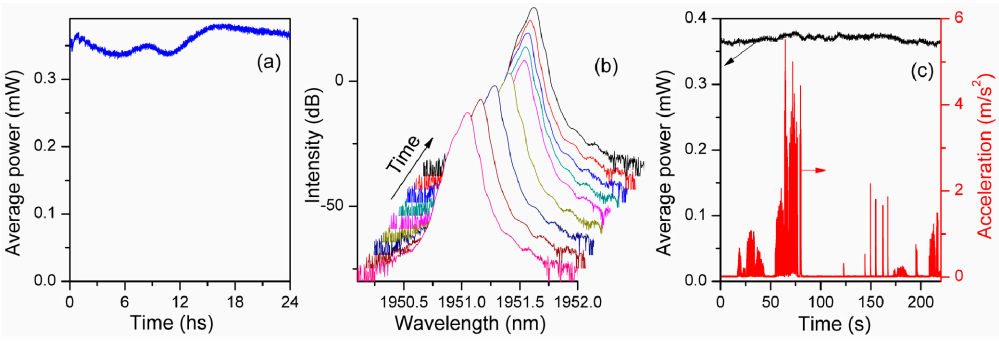

Figure 4. (**a**,**b**) Measured output power and spectrum, respectively, in 24 h operation. (**c**) Measured output power in a simulated harsh environment and acceleration modulus; (left and right ordinates, respectively).

4. Conclusions

In this work, we have compared the passively modelocked polarization-maintaining emission in two thulium-doped fiber lasers with emissions at wavelengths of 1.95 μm in one case and 2.07 μm in the other. The sequence of light pulses was observed at 15.6 MHz (FWHM of 81 ps at 1.95 μm) and at 13.1 MHz (FWHM of 94 ps at 2.07 μm). Since insensitivity to environmental effects, such as thermal fluctuations and vibrations, is very important for practical applications, we also measured the long-term stability of this setup in 24 h operation as well as the short-term stability in a simulated harsh environment. The measured output power and spectrum trends showed that the laser is environmentally stable, not to mention easy to fabricate with commercially available components and compact in design. These characteristics make this proposal a promising candidate for various applications, such as low-latency communications, spectroscopy, LIDAR, and fiber-optic sensing.

Author Contributions: Conceptualization, M.V.A., A.D. and J.L.C.; methodology, M.V.A. and C.C.-L.; investigation, C.C.-L.; resources, J.L.C.; data curation, C.C.-L.; writing—original draft preparation, C.C.-L. and M.V.A.; writing—review and editing, C.C.-L. and M.V.A.; visualization, C.C.-L.; supervision, M.V.A., A.D. and J.L.C.; project administration, M.V.A. and A.D.; funding acquisition, M.V.A. and A.D. All authors have read and agreed to the published version of the manuscript.

Funding: This research was funded in part by the European Union, project IPN-Bio (Ref.: H2020-MSCA-RISE-2019-872049), and by the *Generalitat Valenciana* of Spain (Ref.: PROMETEO/2019/048).

Institutional Review Board Statement: Not applicable.

Informed Consent Statement: Not applicable.

Data Availability Statement: The data presented in this study are available upon reasonable request.

Conflicts of Interest: The authors declare no conflict of interest.

References

1. Rudy, C.W.; Digonnet, M.J.; Byer, R.L. Advances in 2-μm Tm-doped mode-locked fiber lasers. *Opt. Fiber Technol.* **2014**, *20*, 642–649. [CrossRef]
2. Orr, B.J. *Infrared LIDAR Applications in Atmospheric Monitoring*; John Wiley & Sons: Hoboken, NJ, USA, 2017. [CrossRef]
3. Koch, G.J.; Beyon, J.Y.; Gibert, F.; Barnes, B.W.; Ismail, S.; Petros, M.; Petzar, P.J.; Yu, J.; Modlin, E.A.; Davis, K.J.; et al. Side-line tunable laser transmitter for differential absorption LIDAR measurements of CO_2: Design and application to atmospheric measurements. *Appl. Opt.* **2008**, *47*, 944–956. [CrossRef]
4. Bertie, J.E.; Lan, Z. Infrared Intensities of Liquids XX: The intensity of the OH stretching band of liquid water revisited, and the best current values of the optical constants of H_2O(l) at 25 °C between 15,000 and 1 cm^{-1}. *Appl. Spectrosc.* **1996**, *50*, 1047–1057. [CrossRef]
5. Scholle, K.; Lamrini, S.; Koopmann, P.; Fuhrberg, P. 2 μm laser sources and their possible applications. In *Frontiers in Guided Wave Optics and Optoelectronics*; Pal, B., Ed.; INTECH Open Access Publisher: London, UK, 2010; p. 471. [CrossRef]
6. Theisen, D.; Ott, V.; Bernd, H.; Danicke, V.; Keller, R.; Brinkmann, R. CW high power IR-laser at 2 μm for minimally invasive surgery. In *Therapeutic Laser Applications and Laser-Tissue Interactions*; Steiner, R., Ed.; SPIE Optical Society of America: Washington, DC, USA, 2003; Volume 5142, p. 5142_96. [CrossRef]
7. Polder, K.D.; Bruce, S. Treatment of Melasma Using a Novel 1,927-nm Fractional Thulium Fiber Laser: A Pilot Study. *Dermatol. Surg.* **2012**, *38*, 199–206. [CrossRef]
8. Xie, X.; Xu, Q.; Hu, W.; Zhang, W.; Dai, Q.; Chen, J.; Deng, J.; Song, H.-Z.; Wang, S.-X. A Brief Review of 2 μm Laser Scalpel. In Proceedings of the 2020 IEEE 5th Optoelectronics Global Conference (OGC), Shenzhen, China, 7–11 September 2020; pp. 63–67. [CrossRef]
9. Shen, W.; Du, J.; Sun, L.; Wang, C.; Zhu, Y.; Xu, K.; Chen, B.; He, Z. Low-Latency and High-Speed Hollow-Core Fiber Optical Interconnection at 2-Micron Waveband. *J. Light. Technol.* **2020**, *38*, 3874–3882. [CrossRef]
10. Mingareev, I.; Weirauch, F.; Olowinsky, A.; Shah, L.; Kadwani, P.; Richardson, M. Welding of polymers using a 2μm thulium fiber laser. *Opt. Laser Technol.* **2012**, *44*, 2095–2099. [CrossRef]
11. Wang, T.; Ma, W.; Jia, Q.; Su, Q.; Liu, P.; Zhang, P. Passively Mode-Locked Fiber Lasers Based on Nonlinearity at 2-μm Band. *IEEE J. Sel. Top. Quantum Electron.* **2018**, *24*, 1–11. [CrossRef]
12. Wu, Y.; Tian, J.-R.; Dong, Z.; Liang, C.; Song, Y.-R. Generation of Two Dissipative Soliton Resonance Pulses in an All-Anomalous-Dispersion Regime Thulium-Doped Fiber Laser. *IEEE Photon- J.* **2019**, *11*, 1–8. [CrossRef]

13. Wang, Q.; Chen, T.; Li, M.; Zhang, B.; Lu, Y.; Chen, K.P. All-fiber ultrafast thulium-doped fiber ring laser with dissipative soliton and noise-like output in normal dispersion by single-wall carbon nanotubes. *Appl. Phys. Lett.* **2013**, *103*, 011103. [CrossRef]
14. Zhao, J.; Li, L.; Zhao, L.; Tang, D.; Shen, D.; Su, L. Tunable and switchable harmonic h-shaped pulse generation in a 303 km ultralong mode-locked thulium-doped fiber laser. *Photon- Res.* **2019**, *7*, 332–340. [CrossRef]
15. Zhao, J.; Ouyang, D.; Zheng, Z.; Liu, M.; Ren, X.; Li, C.; Ruan, S.; Xie, W. 100 W dissipative soliton resonances from a thulium-doped double-clad all-fiber-format MOPA system. *Opt. Express* **2016**, *24*, 2072–2081. [CrossRef] [PubMed]
16. Ibarra-Escamilla, B.; Duran-Sanchez, M.; Posada-Ramirez, B.; Santiago-Hernandez, H.; Alvarez-Tamayo, R.I.; de la Llave, D.S.; Bello-Jimenez, M.; Kuzin, E.A. Dissipative Soliton Resonance in a Thulium-Doped All-Fiber Laser Operating at Large Anomalous Dispersion Regime. *IEEE Photon- J.* **2018**, *10*, 1503907. [CrossRef]
17. Li, J.; Zhang, Z.; Sun, Z.; Luo, H.; Liu, Y.; Yan, Z.; Mou, C.; Zhang, L.; Turitsyn, S. All-fiber passively mode-locked Tm-doped NOLM-based oscillator operating at 2-μm in both soliton and noisy-pulse regimes. *Opt. Express* **2014**, *22*, 7875–7882. [CrossRef]
18. Du, T.; Li, W.; Ruan, Q.; Wang, K.; Chen, N.; Luo, Z. 2 μm high-power dissipative soliton resonance in a compact σ-shaped Tm-doped double-clad fiber laser. *Appl. Phys. Express* **2018**, *11*, 052701. [CrossRef]
19. Wang, H.W.H.; Du, T.D.T.; Li, Y.L.Y.; Zou, J.Z.J.; Wang, K.W.K.; Zheng, F.Z.F.; Fu, J.F.J.; Yang, J.Y.J.; Fu, H.F.H.; Luo, Z.L.Z. 2080 nm long-wavelength, high-power dissipative soliton resonance in a dumbbell-shaped thulium-doped fiber laser. *Chin. Opt. Lett.* **2019**, *17*, 030602. [CrossRef]
20. Wang, F.; Zhang, X.-L.; Cui, J.-H.; Huang, J.-J. Evolution of Soliton Rain in a Tm-doped Passive Mode-Locked All-Fiber Laser. *IEEE Photon- J.* **2020**, *12*, 1503408. [CrossRef]
21. Luo, Y.; Zhou, Y.; Tang, Y.; Xu, J.; Hu, C.; Gao, L.; Zhang, H.; Wang, Q. Mode-locked Tm-doped fiber laser based on iron-doped carbon nitride nanosheets. *Laser Phys. Lett.* **2017**, *14*, 110002. [CrossRef]
22. Wang, M.; Huang, Y.; Song, Z.; Wei, J.; Pei, J.; Ruan, S. Two-micron all-fiberized passively mode-locked fiber lasers with high-energy nanosecond pulse. *High Power Laser Sci. Eng.* **2020**, *8*, e14. [CrossRef]
23. Wang, X.-F.; Peng, X.-L.; Jiang, Q.-X.; Gu, X.-H.; Zhang, J.-H.; Mao, X.-F.; Yuan, S.-Z. 2-μm mode-locked nanosecond fiber laser based on MoS_2. *Chin. Phys. B* **2017**, *26*, 114205. [CrossRef]
24. Wan, P.; Yang, L.-M.; Liu, J. High power 2 μm femtosecond fiber laser. *Opt. Express* **2013**, *21*, 21374–21379. [CrossRef]
25. Wang, X.-F.; Jin, Z.-G.; Liu, J.-H. 2.04 μm harmonic noise-like pulses generation from a mode-locked fiber laser based on nonlinear polarization rotation. *Optoelectron. Lett.* **2021**, *17*, 18–21. [CrossRef]
26. Cao, R.; Lu, Y.; Tian, Y.; Huang, F.; Xu, S.; Zhang, J. Spectroscopy of thulium and holmium co-doped silicate glasses. *Opt. Mater. Express* **2016**, *6*, 2252–2263. [CrossRef]
27. Khamis, M.A.; Ennser, K. Broadband amplified spontaneous emission thulium-doped fiber sources near 2 μm. In *Horizons in World Physics 299*; Reimer, A., Ed.; Nova Science Publishers: Hauppauge, NY, USA, 2019; Chapter 3.
28. Hemming, A.; Simakov, N.; Haub, J.; Carter, A. A review of recent progress in holmium-doped silica fibre sources. *Opt. Fiber Technol.* **2014**, *20*, 621–630. [CrossRef]
29. Quan, Z.; Gao, C.; Guo, H.; Wang, N.; Cui, X.; Xu, Y.; Peng, B.; Wei, W. 400 mW narrow-linewidth Tm-doped silica fiber laser output near 1750nm with volume Bragg grating. *Sci. Rep.* **2015**, *5*, 12034. [CrossRef] [PubMed]
30. Lee, J.; Lee, J. A Passively Q-Switched Holmium-Doped Fiber Laser with Graphene Oxide at 2058 nm. *Appl. Sci.* **2021**, *11*, 407. [CrossRef]
31. Jackson, S.; King, T. Theoretical modeling of Tm-doped silica fiber lasers. *J. Light. Technol.* **1999**, *17*, 948–956. [CrossRef]
32. Cuadrado-Laborde, C.; Cruz, J.L.; Diez, A.; Andres, M.V. Passively Modelocked All-PM Thulium-Doped Fiber Laser at 2.07 μm. *IEEE Photon- J.* **2022**, *14*, 1539005. [CrossRef]
33. Jackson, S. The spectroscopic and energy transfer characteristics of the rare earth ions used for silicate glass fibre lasers operating in the shortwave infrared. *Laser Photon- Rev.* **2009**, *3*, 466–482. [CrossRef]
34. Available online: https://www.newport.com/t/high-speed-detectors (accessed on 1 October 2022).
35. Sánchez, L.; Cuadrado-Laborde, C.; Carrascosa, A.; Díez, A.; Cruz, J.; Andrés, M. Low-repetition-rate all-polarization maintaining thulium-doped passively modelocked fiber laser. *Opt. Laser Technol.* **2022**, *149*, 107856. [CrossRef]
36. Ahmad, H.; Samion, M.; Kamely, A.; Ismail, M. Mode-locked thulium doped fiber laser with zinc oxide saturable absorber for 2 μm operation. *Infrared Phys. Technol.* **2019**, *97*, 142–148. [CrossRef]
37. Martínez, O.E.; Fork, R.L.; Gordon, J.P. Theory of passively mode-locked lasers including self-phase modulation and group-velocity dispersion. *Opt. Lett.* **1984**, *9*, 156–158. [CrossRef] [PubMed]
38. Haus, H. Mode-locking of lasers. *IEEE J. Sel. Top. Quantum Electron.* **2000**, *6*, 1173–1185. [CrossRef]
39. Afkhamiardakani, H.; Tehrani, M.; Diels, J.-C. Extension of the stable operation of an all polarization maintaining mode-locked fiber laser. In Proceedings of the Conference on Lasers and Electro-Optics, OSA Technical Digest. Online, 13–18 May 2018; p. JTh2A.141.

40. Zhang, Y.; Zheng, Y.; Su, X.; Peng, J.; Yu, H.; Sun, T.; Zhang, H. All-Polarization Maintaining Noise-Like Pulse From Mode-Locked Thulium-Doped Fiber Laser Based on Nonlinear Loop Mirror. *IEEE Photon- J.* **2022**, *14*, 1–5. [CrossRef]
41. Shen, X.; Li, W.; Zeng, H. Polarized dissipative solitons in all-polarization-maintained fiber laser with long-term stable self-started mode-locking. *Appl. Phys. Lett.* **2014**, *105*, 101109. [CrossRef]
42. Zhang, L.; Zhou, J.; Wang, Z.; Gu, X.; Feng, Y. SESAM Mode-Locked, Environmentally Stable, and Compact Dissipative Soliton Fiber Laser. *IEEE Photon- Technol. Lett.* **2014**, *26*, 1314–1316. [CrossRef]